The third integral in Eq. (2.3) is the contribution from the wake surface. Here, the upper and lower surfaces have been combined, taking the upward facing normal. The upper and lower potentials have been combined, yielding a wake doublet distribution of strength,

$$\mu_W = \frac{(\phi_U - \phi_L)}{4\pi} \tag{2.6}$$

This is the potential jump across the wake. In combining the upper and lower surfaces, the source term has been discarded, implying that there is no normal flow relative to the wake--the wake points, in fact, convect with the flow and so the wake surface is always aligned with the local flow. (The entrainment effect due to turbulent mixing is neglected for the moment.) Thus, Eq. (2.3) becomes

$$\iint_{S-P} \mu\, \vec{n} \cdot \nabla\left(\frac{1}{r}\right) dS - 2\pi\mu_p + \iint_S \frac{\sigma}{r}\, dS + \iint_W \mu_W \vec{n} \cdot \nabla\left(\frac{1}{r}\right) dW = 0 \tag{2.7}$$

In the general case of analyzing the flow about a given configuration, the doublet distribution on the surface is unknown, while the source distribution is determined directly by the external Neumann boundary condition specifying the resultant normal velocity at the boundary. The flow velocity relative to the surface is

$$\vec{V} = \vec{v} - \vec{V}_s \tag{2.8}$$

where $\vec{v}$ is the perturbation velocity (eq. (2.2)), and

$$\vec{V}_s = \vec{V}_B + \vec{\Omega} \times \vec{R} - \vec{V}_\infty \tag{2.9}$$

is the surface velocity relative to the undisturbed fluid. V_B is now measured in an inertial frame which may have a uniform flow, V_∞. $\vec{\Omega}$ is the velocity of rotation of the body, and $\vec{R}$ the position of a surface point relative to the rotational axis. The normal component of $\vec{V}$ is, from Eq. (2.8),

$$\vec{V} \cdot \vec{n} = \vec{v} \cdot \vec{n} - \vec{V}_s \cdot \vec{n} = V_N \tag{2.10}$$

V_N is the resultant normal velocity at the surface. This is usually zero (solid boundary), but it can have a number of nonzero parts, e.g.,

$$V_N = VNORM + V_{BL} \tag{2.11}$$

where VNORM is the user-specified inflow/outflow representing an engine inlet/exhaust modeling, and V_{BL} is the boundary layer displacement effect using the transpiration technique,

$$V_{BL} = \frac{\partial}{\partial s}(V_e \delta^*) \tag{2.12}$$

where V_e is the local speed at the edge of the boundary layer and δ^* is the displacement thickness. The derivative is taken in the direction of the local external flow.

Using Eqs. (2.2), (2.5) and (2.10), the source term is,

$$\sigma = \frac{\left(\vec{n} \cdot \vec{V}_B + \vec{\Omega} \cdot \vec{R} \wedge \vec{n} - \vec{n} \cdot \vec{V}_\infty + VNORM + V_{BL}\right)}{4\pi} \tag{2.13}$$

The wake doublet distribution, μ_w, in Eq. 2.7, is treated differently in the two codes: in VSAERO, μ_w, is constant along streamlines in the wake surface. The value of μ_w on each streamline takes the difference in strength between the upper and lower solid surface doublet values where the streamline leaves the trailing edge. In this case, μ_w becomes involved with the *unknown* surface-doublet distribution. In USAERO, the wake doublet distribution is essentially *known* from earlier time steps: as each new wake element is created, it carries with it the instantaneous doublet jump at the local trailing edge, and holds this constant for the rest of the calculation.

2.4 Surface Pressure

With the solution known, the surface velocities and pressures can be evaluated. The tangential component of perturbation velocity is obtained from the surface gradient of the potential. The normal component comes from the source term. The pressure is evaluated using the Bernoulli equation for a moving frame,

$$C_p = V_s^2 - V^2 + 2\left(\frac{\partial \phi}{\partial \tau}\right). \tag{2.14}$$

In VSAERO, the $\frac{\partial \phi}{\partial \tau}$ term is zero. The velocities V_s, V, are normalized by the reference speed; this may be the blade tip speed or it may be the local speed due to rotation at the local radius.

2.5 Kutta Condition

In VSAERO, the (steady state) Kutta condition is usually satisfied implicitly by shedding the doublet jump across the trailing edge into the local wake column,

$$\mu_W = \mu_U - \mu_L \tag{2.15}$$

This essentially states that there is zero load at the trailing edge.

An iterative loop is available in the code for explicitly satisfying a zero pressure jump condition at the trailing edge; however, it was not applied in the present cases.

In USAERO, an *unsteady* Kutta condition is obtained after equating the unsteady upper and lower trailing edge pressures using the C_P expression in Eq. (2.14):

$$\left(\frac{\partial \mu_W}{\partial \tau}\right) + V_M\left(\frac{\partial \mu_W}{\partial s}\right) = 0 \tag{2.16}$$

V_M is the mean convection speed and the s direction follows the local mean flow at the trailing edge. μ_W is the jump in doublet strength across the trailing edge, i.e., μ_W is the newly emerging wake strength. Equation (2.16) essentially states that the rate of change of circulation at the trailing edge must match the transport of circulation into the wake.

2.6 Force and Moment

The forces and moments are obtained by integrating the pressure over the surface.

The force coefficient is,

$$\vec{C}_F = -\iint_S C_p \vec{n} - C_f \vec{V}_R |\vec{V}R| dS \tag{2.17}$$

The moment coefficient is,

$$\vec{C}_M = \iint_S \left(Cp\vec{n} - C_f \vec{V}_R |\vec{V}_R|\right) \times \vec{r}\, dS \tag{2.18}$$

The axial components of these quantities provide the thrust and torque values, respectively, for a propellar configuration.

3.0 NUMERICAL PROCEDURE

3.1 General

The numerical procedure flow diagrams for VSAERO and USAERO are shown in Fig. 3.1. The main difference is that the separate iteration loops for spatial wake relaxation and steady boundary layer effects in VSAERO become a single in-line time-step loop in USAERO with time-domain wake convection and unsteady integral boundary layer treatment.

The *initial set-up* is very similar in the two codes and involves the specifications of *basic data* such as onset conditions, reference quantities, program controls, etc. VSAERO uses fixed format for this input, whereas USAERO now has a *namelist* style of input format; the namelist scheme was written specifically for the code in standard Fortran 77 and is therefore portable to a wide range of computers.

The *geometry definition* involves the description of the *configuration* surfaces. Both VSAERO and USAERO provide the option to break the configuration into a number of convenient parts. USAERO, in addition, allows the user to specify multiple moving frames of reference. Configuration modeling aspects are discussed below in Section 3.2. The smallest subdivision of a configuration surface is a quadrildial *panel*. Panels are arranged in a structured mesh of rows and columns and are the basic elements used to discretize Eq. (2.7). These aspects and the formation of the *matrix of influence coefficient* are discussed in 3.3; *matrix solution* options are given in 3.4. *Analysis* of the surface velocities and pressures, and the treatment of the surface streamlines, boundary layers and wakes, are outlined in 3.5, 3.6., 3.7 and 3.8, respectively.

3.2 Configuration Modeling

Configuration refers to the vehicle, bodies, etc. and their wakes about which the flow is to be calculated. It includes all solid boundaries in the flow problem; for example, a *configuration* may include the wind tunnel walls or water tank walls in cases where model test measurements are being used to validate calculations. The present section is concerned with creating a panel model, which represents the *configuration surfaces* in the flow calculations. Treatment of a *configuration* in USAERO is basically similar to that in VSAERO, except there is now an additional breakdown level, i.e., *frames*. These provide a convenient way of describing arbitrary movements of multiple parts of the vehicle.

Fig. 3.2 shows the breakdown of a *configuration* into a number of convenient parts, i.e., *frames, components, patches, panels,* and *wakes*. The first step in breaking down a *configuration* into manageable pieces is to identify the individual motions of its various parts. This establishes the *frames* of reference required to describe the various motions. *Configuration* parts associated with each *frame* may consist of one or more *components*. The *component* breakdown is chosen by the user on the basis of convenient parts for separate force and moment information; for example, a hull, a blade stator or duct, etc. In USAERO, each *component* is assigned to a *frame*--this is its local reference frame in which its basic geometry is first described. If the *component* has no motion, it may be assigned directly to the ground-fixed frame.

A *component* is further subdivided into one or more *patches*. The *patch* breakdown is selected with a view to paneling convenience, or available section geometry information. A surface *patch* consists of a set of ***panels*** arranged in a structured network of rows and columns.

Careful attention to the details of panel arrangement over the configuration surface helps ensure a good quality solution, particularly in regard to the evaluation of doublet gradients (i.e., tangential velocity components). Both programs provide various automatic paneling options to help the user distribute the panels over each patch.

Lines of wake separation are identified on the configuration surfaces. Each wake is assigned to the patch where it leaves the surface. Multiple wake/patch assignments are allowed to cover the case where a wake separation line extends over more than one patch.

3.3 Matrix Equations

The surface integrals in Eq. (2.7) are evaluated in a piecewise manner over each panel assuming the doublet and source are locally uniform. In USAERO, the doublet distribution on each wake panel is assumed to be linear in the streamwise direction and the integration is performed over a pair of triangles in order to treat the possibly highly warped quadrilaterals in a strong wake roll-up situation. The piecewise integration yields influence coefficients for source and doublet singularities (1) and Eq. (2.7) becomes,

$$\sum_{K=1,K\neq J}^{N_e} (\mu_K C_{JK}) - 2\pi\mu_J + E_J = 0 \qquad J=1,N \tag{3.1}$$

where μ_K is the doublet value for panel K and C_{JK} (1) is the doublet influence coefficient for panel K acting at the control point of panel J.

$$E_J = \sum_{K=1}^{N_s} \sigma_K B_{JK} + \sum_{K=1}^{N_W} \mu_{WK} C_{JK} \tag{3.2}$$

N_s is the number of surface panels and N_w the number of wake panels.

B_{JK} is the source influence coefficient for panel K acting at the central point of panel J.

C_{JK} and B_{JK} are given in Ref. 1 and include symmetry terms for configurations having geometrical and aerodynamic symmetries.

In USAERO, surface panels involved with wake shedding have a small contribution from the newly formed wake panel. Basically, the doublet value at the downstream edge is the value propagated at the last time step. At the upstream edge, i.e., at the shedding line, the doublet strength is unknown. The influence coefficient for these wake panels, therefore, goes partly into the known right-hand side of the equations and partly into the matrix of influence coefficients to contribute to the "upper" and "lower" wake-shedding panels, see Fig. 3.3.

In VSAERO, the influence coefficient for a complete streamline set of wake panels is combined with the influence coefficients of the wake-shedding panels, being added to the "upper" and subtracted from the "lower" term.

3.4 Matrix Solution

Both codes offer a number of matrix solver options which may be selected at the input stage. A blocked Gauss-Seidel iterative method and the direct Purcell vector method (for smaller problems) are the basic solvers in each code. An alternative special solver was developed in USAERO to deal with problems having *relative* motions. This method reorders the matrix at each time-step if necessary, based on a panel proximity criterion; this condenses the major terms towards the matrix diagonal. A direct solution is then obtained for the banded matrix using a band width of the order of 100. A Jacobi iteration on the complete matrix with further banded matrix treatment of the residuals provides a fairly robust iterative solver for complex configurations.

Other solver options point to various in-core solvers that have been optimized for specific computers. For example, the LAPACK (direct) solver on the Silicon Graphics workstation has shown a 3:1 speedup over the Purcell vector method. *Direct* solutions for 10,000 panels have been executed in a reasonable time scale using a Convex C.3 in-core solver.

3.5 Surface Pressure Analysis

The surface gradient of the potential is evaluated at the center of each panel by differentiating a two-way parabolic curve fit through the values on the panel and its four immediate neighbors. At certain lines on the surface where there is a jump in conditions, e.g., a wake separation line, the code uses forward or backward differencing using information from a neighbor of a neighbor if available. The surface gradient of the potential provides the tangential perturbation velocity while the normal perturbation velocity comes from the source term. There are combined with the local "body" velocity to provide the total fluid velocity relative to the surface point, Eq. (2.8). The pressure coefficient is then evaluated at each panel center (Eq. (2.14)). The $\partial\phi/\partial\Upsilon$ term for USAERO is evaluated using second order differencing based on the two previous time steps.

3.6 Surface Streamlines

With the surface flow velocities known, families of streamlines (instantaneous in the case of USAERO) are traced over the configuration by an automatic integration process. These provide a basis for 2-D integral boundary layer calculations (outlined below). This approach has been successfully applied to a wide range of very complex problems and provides a more versatile and robust alternative to fully 3-D boundary layer methods.

3.7 Boundary Layer Analysis

In the VSAERO boundary layer routines, the laminar calculation is based on Curle's method (2). Once transition or laminar separation is detected (by a modified Granville approach), or boundary layer tripping is prescribed, the turbulent boundary layer development is determined by a modified Nash and Hicks method (3).

In USAERO laminar boundary layer calculations follow Curle's original Method (2) with modification to solve the unsteady momentum integral equation using a Runge-Kutta method. The turbulent boundary layer method is also based on the unsteady momentum integral equation. Cousteix's entrainment relation (4) and Lyrio/Ferziger's skin friction relationship (5) are used for closure. The details of the method are described in Ref. 6.

The calculations provide the boundary layer displacement source term and skin friction distribution along each of the instantaneous streamlines. These quantities are then redistributed onto the surface panels in the attached flow regions. The skin friction force contribution is included in the analysis of forces and moments. The calculations also provide the location of separation on each streamline, based on a vanishingly small skin friction coefficient. The locus of such points defines a separation line on the body surface. At this time there is no automatic coupling of these data with the wake shedding routine. Simple cases of separated flow can be treated, but the user must specify the separation line at this time, based on the boundary layer prediction.

3.8 Wake Treatment

In VSAERO, there is an option to iteratively relax the wake surfaces into a force-free condition by aligning each individual wake longitudinal segment (Fig. 3.3) into the local flow direction. The latter is computed by summing the velocity influences of all the source and doublet singularity panels on the configuration and its wake, including *image* contributions if planes of symmetry are being used or if anisymmetric conditions for multiple propeller blades exist.

The force-free wake condition in USAERO is satisfied by convecting each free wake point along the instantaneous local computed velocity vector for the duration of the time step. A new set of wake points is therefore created along the wake-shedding lines at each time step. Each new wake point is given a doublet value equal to the difference in doublet strength between the local upper and lower wake shedding panels. This value remains constant for each wake point as it convects downstream. In this way, the *vorticity* on the wake varies in time and space according to the local stretching or contraction of the wake surface as the wake points convect at different rates and in different directions.

4.0 CALCULATIONS

4.1 Three-Bladed Propeller, DTRC 42119

4.1.1 Panelling

The panelling used for the DTRC 4119 propeller is shown in Fig. 4.1. The total number of unknowns is 1755 with 900 on the blade in a 60 (around the chord) x 15 (radial) array and 855 on the hub. The computing time for VSAERO/MPROP with rigid wake was 388 seconds on an SGI 4D/35 personal IRIS workstation. The time-stepping calculations in USAERO with free wake analysis "converged" to steady state in about 13 steps in a time of 4725 seconds.

4.1.2 Pressure Distribution

Fig. 4.2(a) shows the pressure coefficient contours computed by VSAERO/MPROP at J = 0.833.

$$(Cp = p - p\infty) / 1/2\rho V_{TIP}^2)$$

Fig. 4.2 (b) shows the "converged" Cp contours predicted by USAERO. Also shown are the computed wake panels, generated in 20 time steps.

Fig. 4.3 shows the USAERO pressure distribution at three radial stations compared with measured data. Here the Cp was reduced (outside the code) to the required form

$$C_p = 1 - (VV/VR)^2$$

The comparison is good at the two inner stations but not at the outer station. The latter problem is being examined further, but it is thought to arise from the form of the panelling in the tip region which has extremely skewed triangular panels.

The corresponding VSAERO Cp plots were not reduced to this form, but a comparative constant radius Cp plot between USAERO and VSAERO indicates very similar solutions (Fig. 4.4). The strange behavior near the trailing edge is partly due to the way the blunt trailing edge region was modified to make it sharp. Fig. 4.5 shows the modified contour detail--this should have been carried over a broader region.

4.1.3 Thrust and Torque

Fig. 4.6(a) shows the KT, KQ curves computed by VSAERO/MPROP. These are for the inviscid case, but no significant change was seen with the boundary layer calculation included. The KT is in very close agreement with experiment while KQ is somewhat low compared with experiment. Computed values at the 0.5 advance coefficient were omitted because of inconsistent behavior in the tip region. Repanelling to avoid the highly skewed triangular tip panels needs to be done before reexamining the lower advance coefficients. This would also allow a more non-linear tip wake model to be examined for possible tip leading edge separation treatment.

The corresponding KT, KQ comparisons for USAERO are shown in Fig. 4.6 (b). The boundary layer effects here are quite significant and in view of the VSAERO/MPROP solutions - need further investigation. The final KT curve is in close agreement with measurement while the total viscous correction to the KQ curve has tended to undershoot the measurement. A large part of the shift probably comes from a reduction in the induced torque due to the large shift in KT at the lower advance coefficients.

4.1.4 Skin Friction Distribution

Fig. 4.7(a) shows the computed skin friction coefficient distribution along streamlines predicted by VSAERO/MPROP for the J = 0.833 case. A significant amount of laminar flow is indicated across the chord at all radial stations. The corresponding calculation in USAERO Fig. 4.7 (b) gives similar behavior in the inner region but indicates earlier transition in the tip region. This solution may have been affected by the unsatisfactory tip panelling noted above.

4.2 Five-Bladed Propeller, DTRC 4842

4.2.1 Panelling

The panelling used for the DTRC 4842 propeller is shown in Fig. 4.8. This has 1550 unknowns with 950 on a blade and 600 in the hub. Computing times for VSAERO/MPROP with rigid wake was 482 seconds on the SGI 4D/35 personal IRIS workstation. USAERO, with free wake calculation converged in about 17 steps in a time of 7320 seconds.

4.2.2 Pressure Distribution

Fig. 4.9(a) shows the pressure coefficient contours $(Cp = p - p_\infty)/1/2\rho V_{TIP}^2)$ computed by VSAERO/MPROP at J = .905. The USAERO solution is shown in Fig. 4.9(b) and includes the computed wake panels for 29 steps.

Fig. 4.10 shows the USAERO pressure distributions at three radial stations. The problems seen in the tip region of DTRC 4119 are not evident here, the panelling form at the tip being less severe on the 5 blader. Also, the behavior near the trailing edge appears much smoother - in this case the modification to sharpen the otherwise blunt trailing edge is taken over a wider region (Fig. 4.11).

4.2.3 Thrust and Torque

Fig. 4.12 shows the KT, KQ curves computed by VSAERO/MPROP compared with experiment and indicate about a 10% difference. Again, no significant viscous correction was shown by VSAERO for this case. USAERO was run only at J = .905 for this case and gave the following results:

	KT	10 x KQ
Experiment	.310	.720
No BL	.359	.6993
With BL	.349	.7397
With BL/No Hub	.352	.7465

Again, USAERO indicates a larger viscous correction than VSAERO. In the present case, this is just due to skin friction. The source term for displacement effect gave a problem on this configuration and was temporarily deactivated.

4.2.4 Skin Friction Distribution

Fig. 4.13(a) shows the VSAERO/MPROP computed skin friction distribution along streamlines for DTRC 4842 at J = .905. Again, VSAERO indicates a significant extent of laminar flow extending right out to the tip. The corresponding calculation in USAERO, Fig. 4.13(b) indicates a region of earlier transition in the middle of the blade. This is more clearly seen in Fig. 4.13(c) which gives the same information transferred to the panels and displayed as contours.

5.0 CONCLUSION

The (steady) VSAERO/MPROP and (unsteady) USAERO codes were applied to the DTRC 4119 and DTRC 4842 propellers with very encouraging results on the whole. Some additional investigation is needed for the panelling details in the tip region of DTRC 4119; USAERO did not behave well near the tip and the VSAERO solution gave spurious results at the lower advance coefficient. The viscous effects also need further examination: whereas the VSAERO calculations showed very small viscous corrections the USAERO calculation indicated significant effects when the boundary layer was activated.

Application of an *unsteady* code to a steady axisymmetric propeller condition in one sense is overkill; the computer time to convergence is about 15 times that required for the steady code. (Even so, the times were not unreasonable, i.e., two hours on an SGI personal IRIS.) The calculations were included here primarily with a view to the more general options provided by the unsteady formulation--viz, non-uniform flows, propeller/hull interaction, variable pitch propellers, etc.

6.0 REFERENCES

1. Maskew, B., "Program VSAERO Theory Document", NASA CR-4023, 1985.
2. Curle, H., "A Two-Parameter Method for Calculating the Two-Dimensional Incompressible Laminar Boundary Layer", J. R. Aero. Soc., Vol. 71, 1967.
3. Nash, J.F. and Hicks, J.G., "An Integral Method Including the Effect of Upstream History on the Turbulent Shear Stress", Proc. Computation of Turbulent Boundary Layers--1968, AFOSR-IFP-Stanford Conference, Vol. 1, 1968.
4. Cousteix, J., and Houdeville, R., "Singularities in Three-Dimensional Turbulent Boundary Layer Calculation and Separation Phenomena", *AIAA J.*, Vol. 21, No. 4, April 1983.
5. Lyrio, A.A., and Ferziger, J.H., "A Method for Predicting Unsteady Turbulent Flows and its Application to Diffusers with Unsteady Inlet Conditions", *AIAA J.*, Vol. 21, No. 4, April 1983.
6. Maskew, B. and Dvorak, F.A., "Prediction of Dynamic Stall Characteristics Using Advanced Nonlinear Panel Methods", presented at AFOSR/FJSRL Workshop on Unsteady Separated Flows, USAF Academy, Colorado Springs, CO, August 1983.

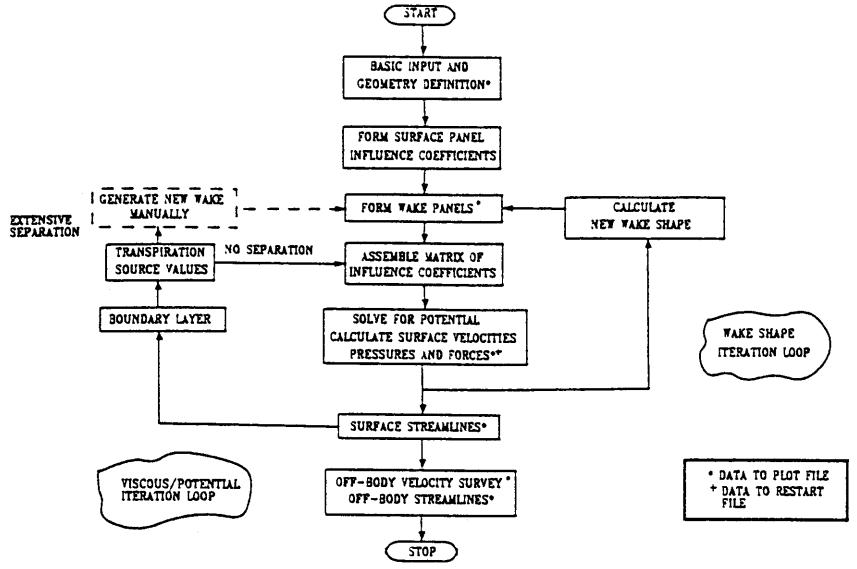

VSAERO

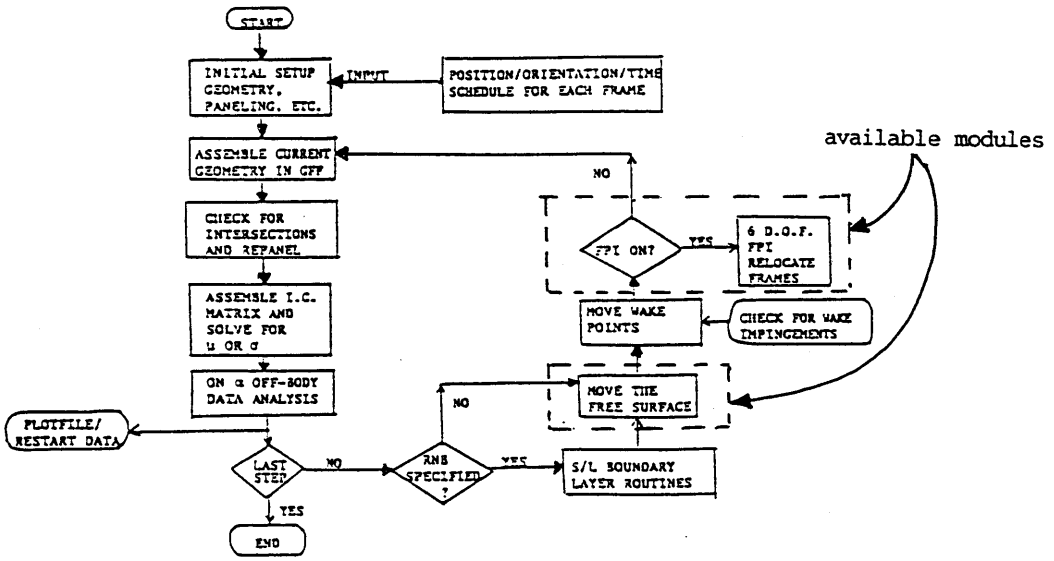

USAERO

Fig. 3.1. Numerical Procedure Flow Diagrams for VSAERO and USAERO

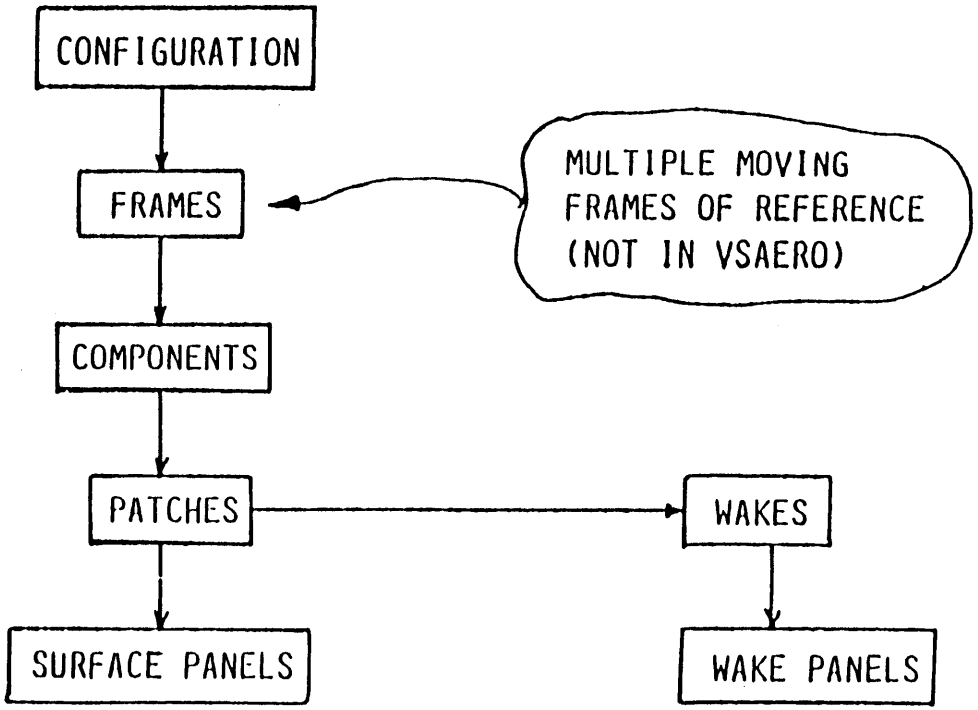

Fig. 3.2. Configuration Breakdown.

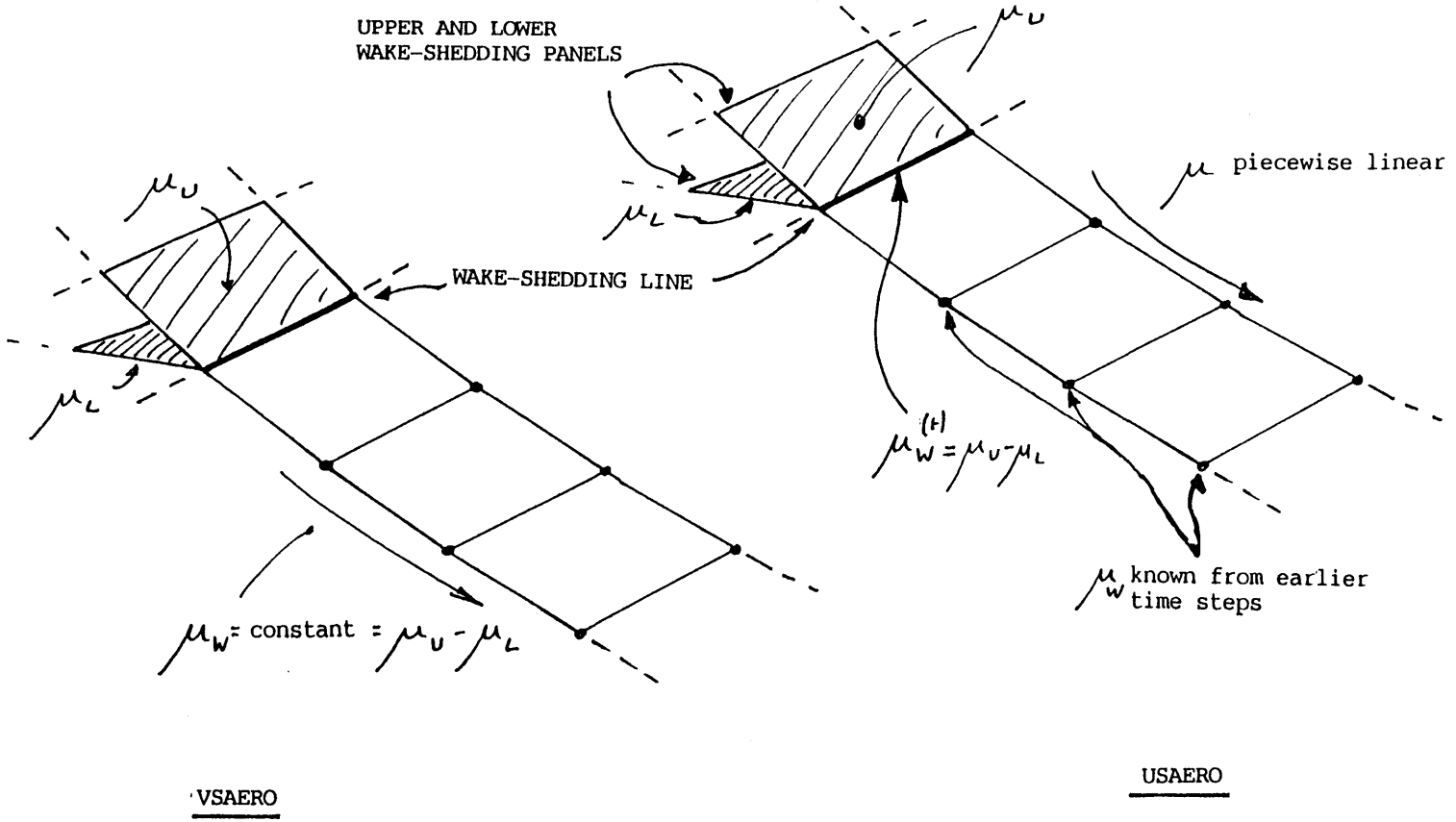

Fig. 3.3. Comparison of Basic Wake Models in VSAERO and USAERO

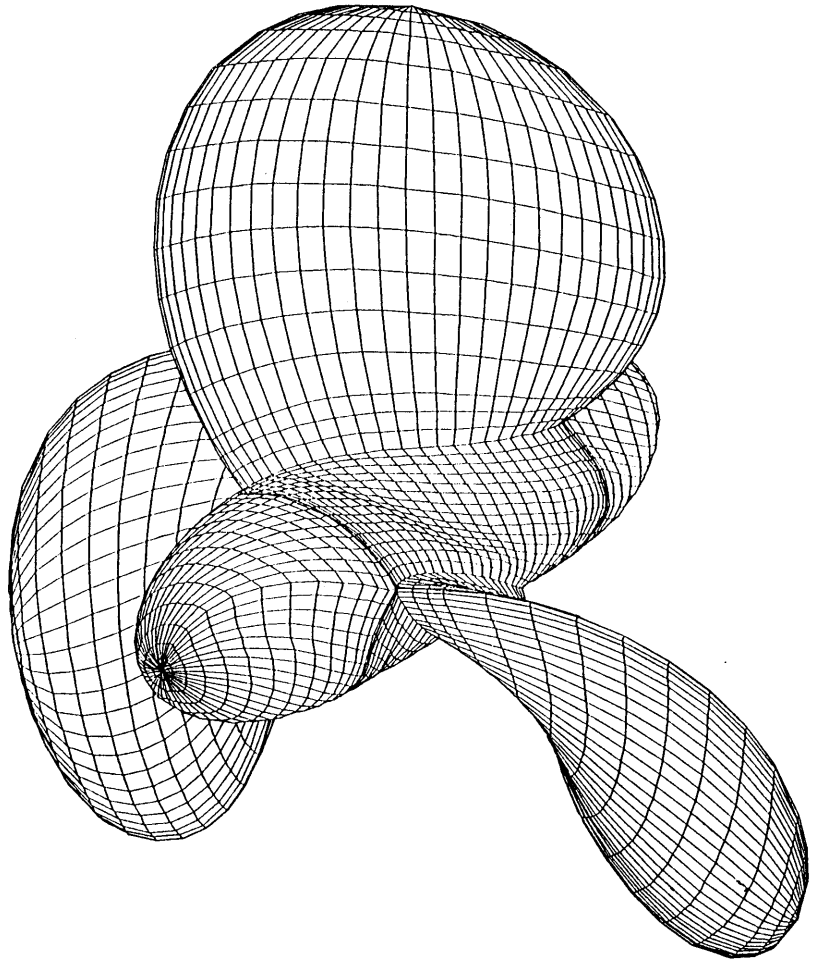

3 BLADE OPEN PROP, DTRC 4119

Fig. 4.1. General View of Panelling

Fig. 4.2. Calculated Pressure Contours at J = .833
(a) VSAERO/MPROP

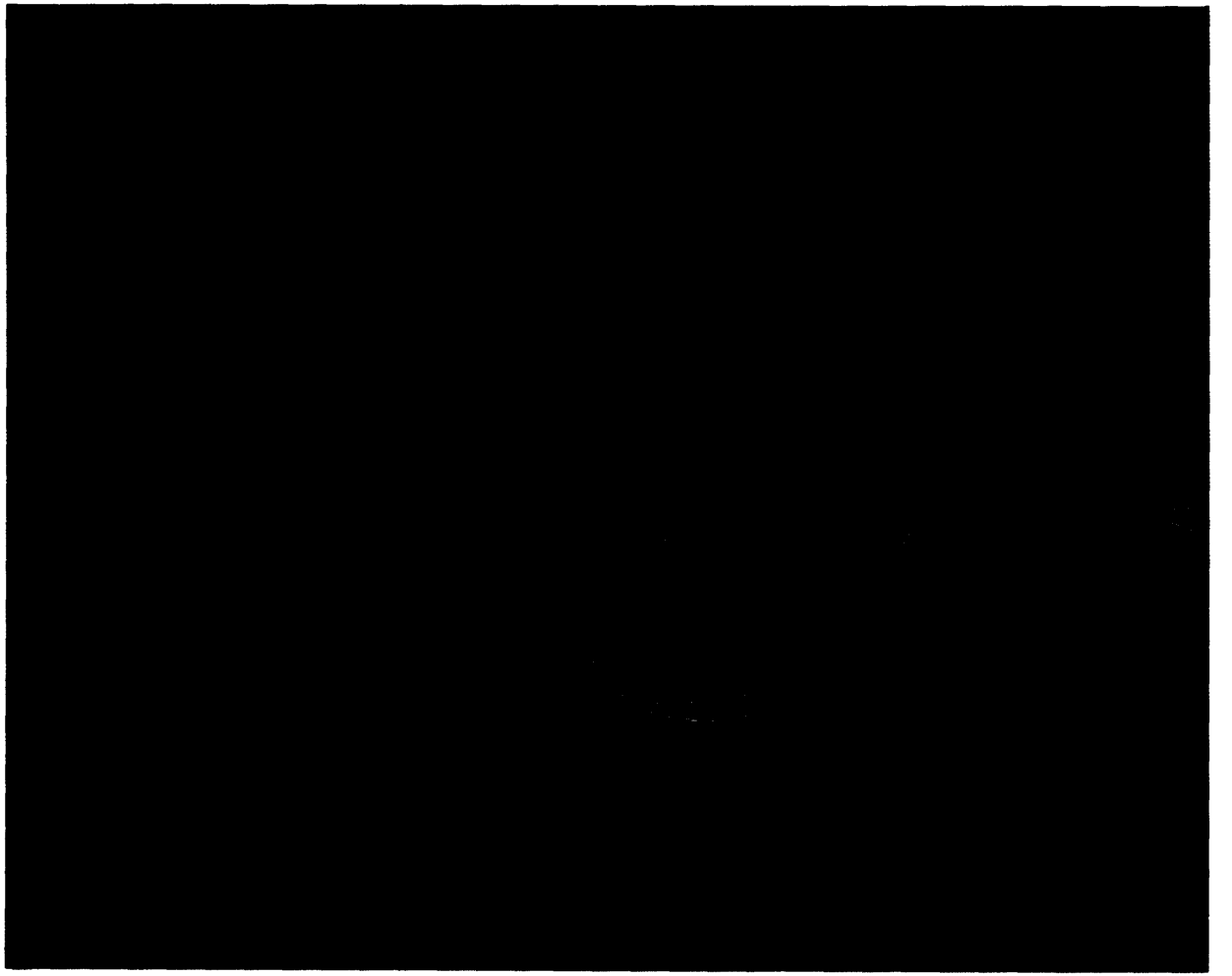

Fig. 4.2. Concluded
(b) USAERO

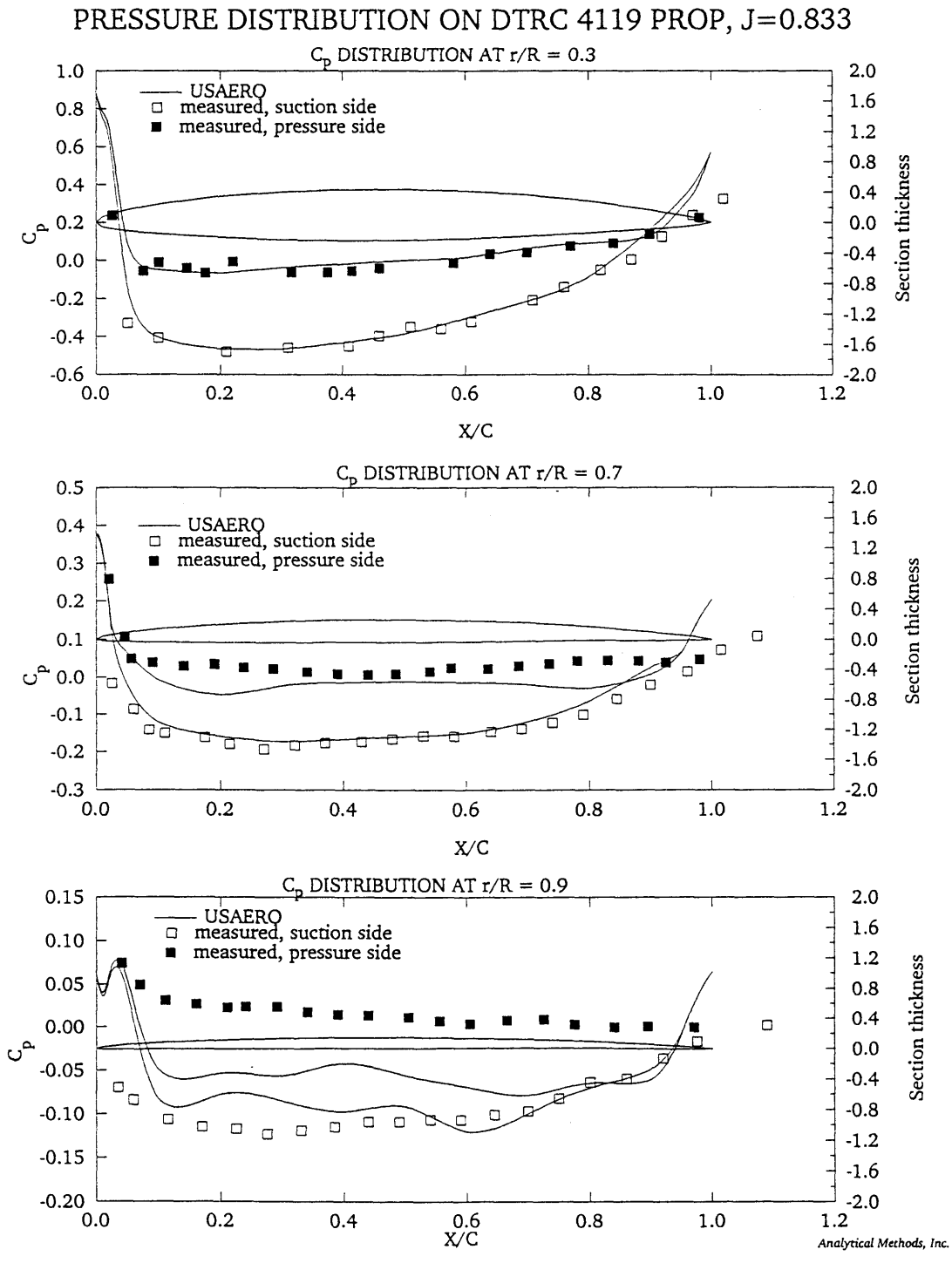

Fig. 4.3. Comparison of USAERO Calculated and Measured Pressure Distributions at Three Radial Stations.

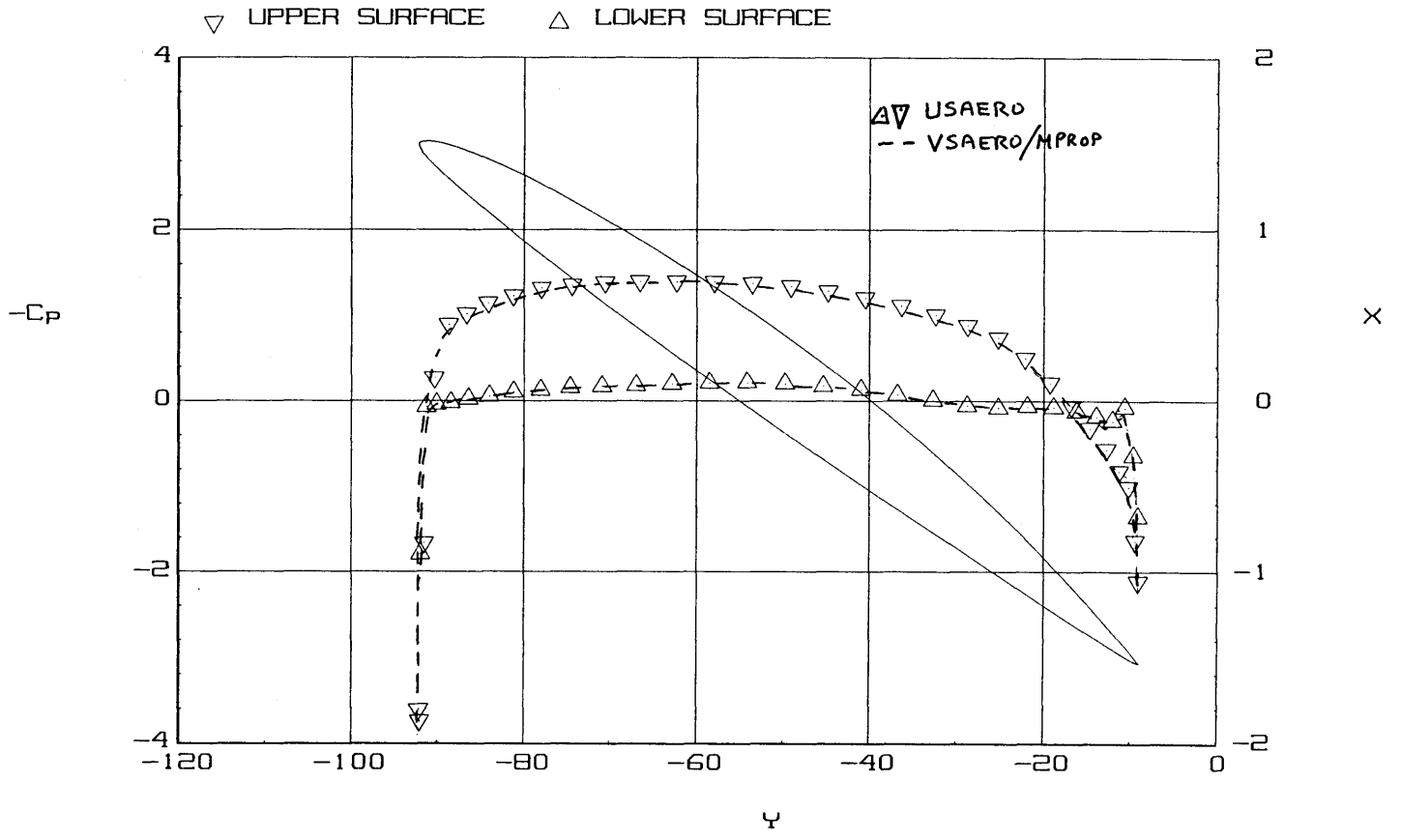

Fig. 4.4. Comparison of VSAERO/MPROP and USAERO Chordwise Pressure Distribution.

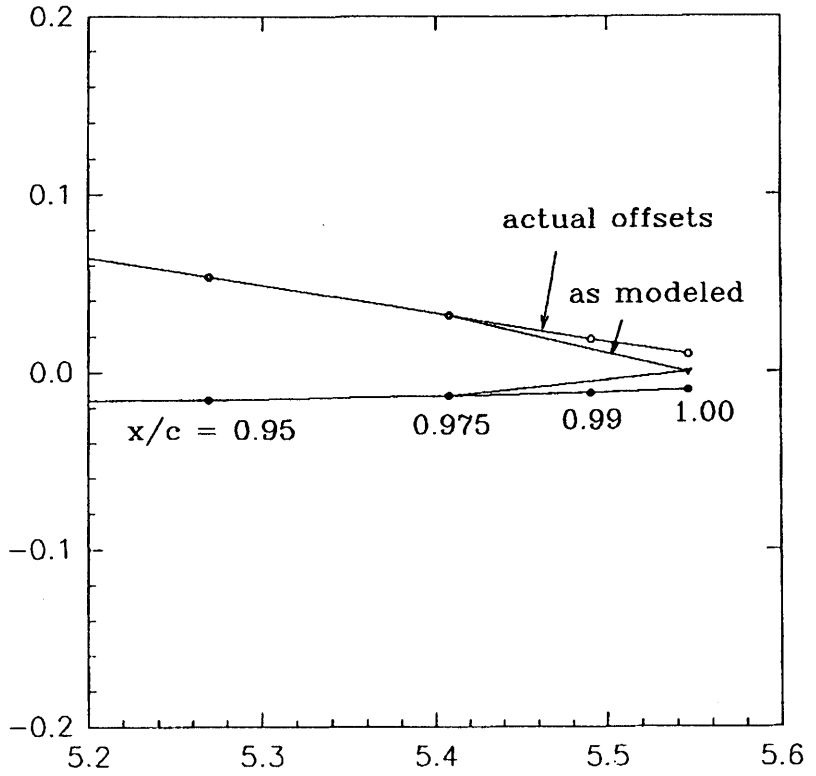

Fig. 4.5. Details of Trailing Edge Modification to Achieve Sharpe Edge.

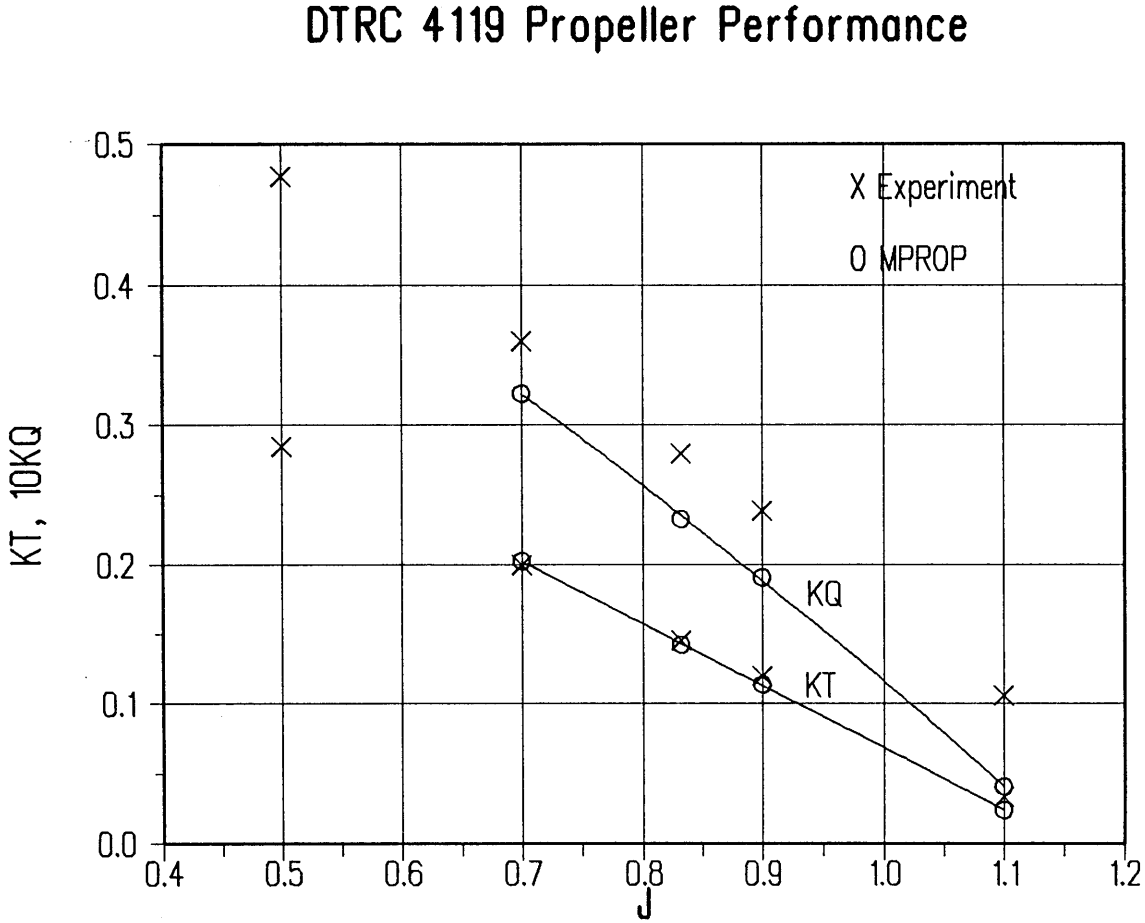

Fig. 4.6. Comparison of Calculated and Measured KT, KQ Characteristics
(a) VSAERO/MPROP

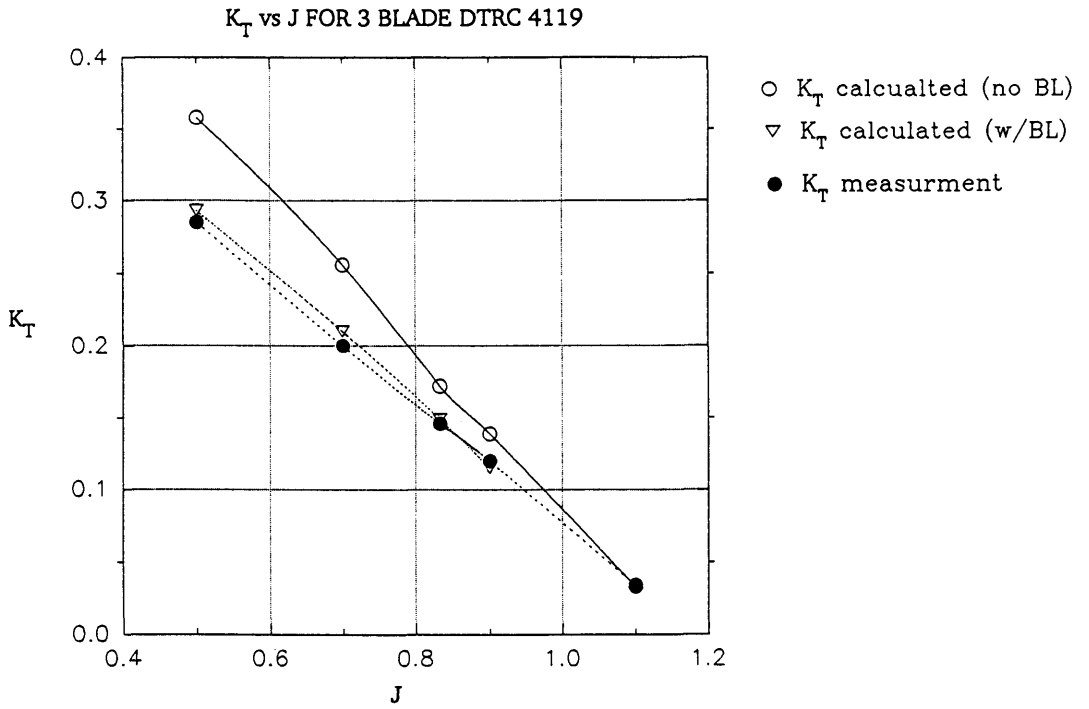

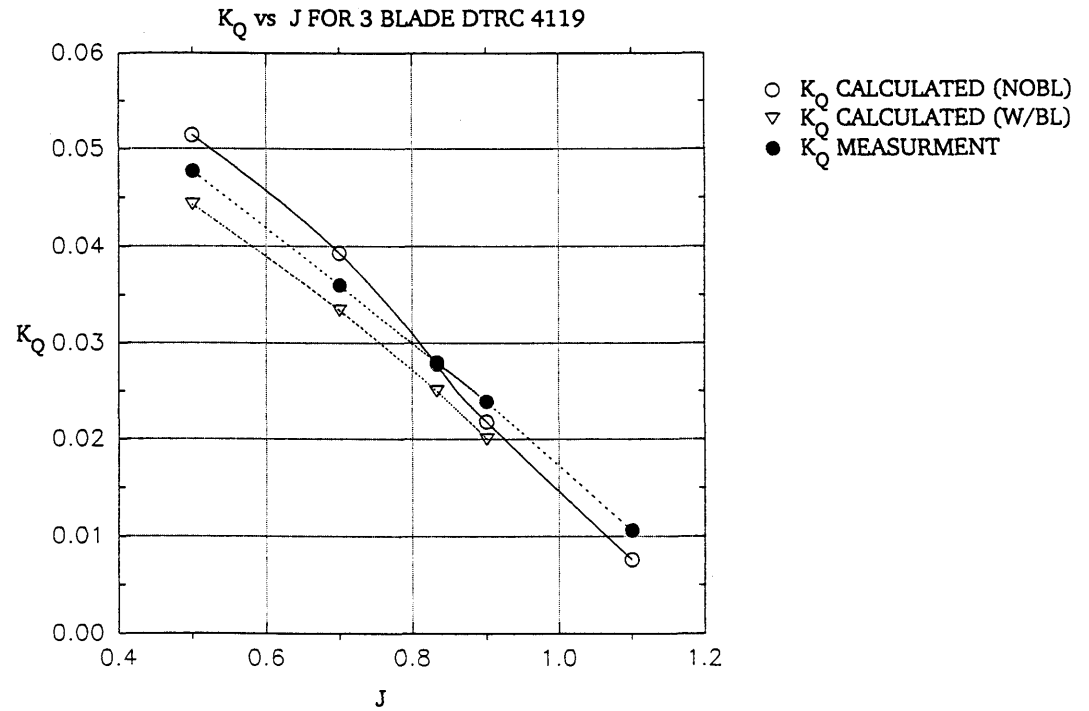

Fig. 4.6. Concluded.
(b) USAERO

Fig. 4.7. Calculated Skin Friction Distribution Along Streamlines at J = 0.833
(a) VSAERO/MPROP

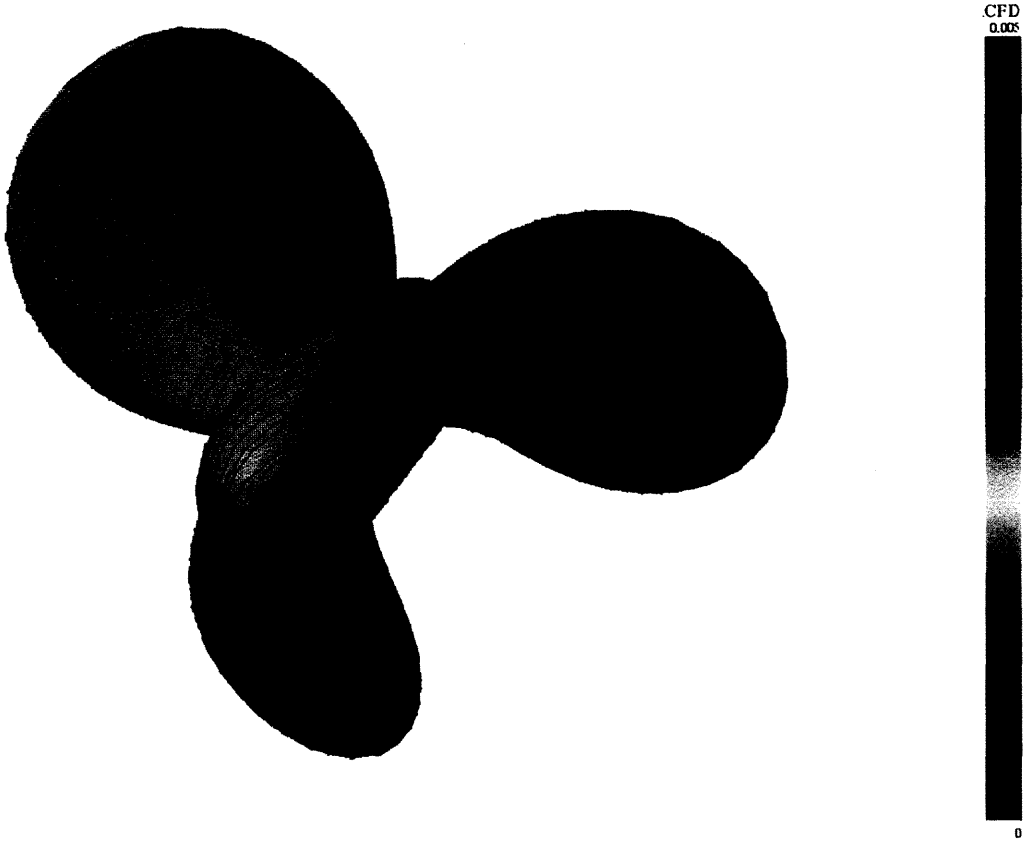

Fig. 4.7. Concluded.
(b) USAERO

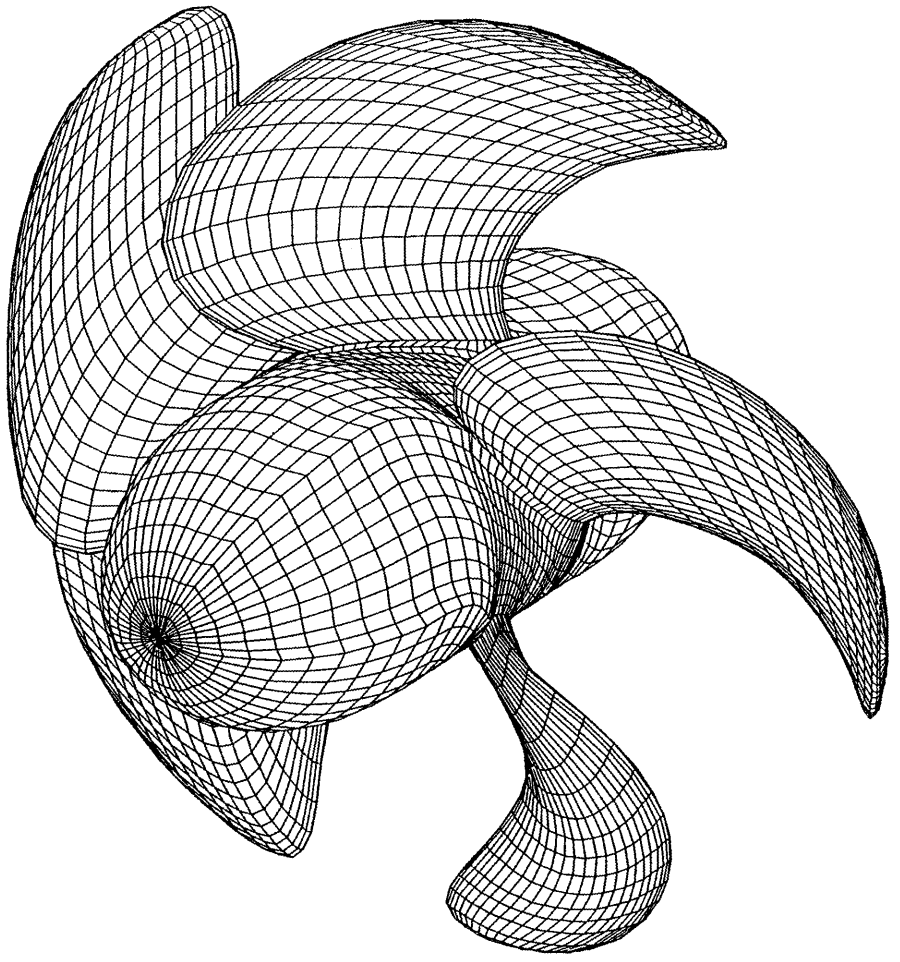

5 BLADE OPEN PROP, DTRC 4842

Fig. 4.8. General View of Panelling

Fig. 4.9. Calculated Pressure Contours at J = 0.905
(a) VSAERO/MPROP

Fig. 4.9. Concluded.
(b) USAERO

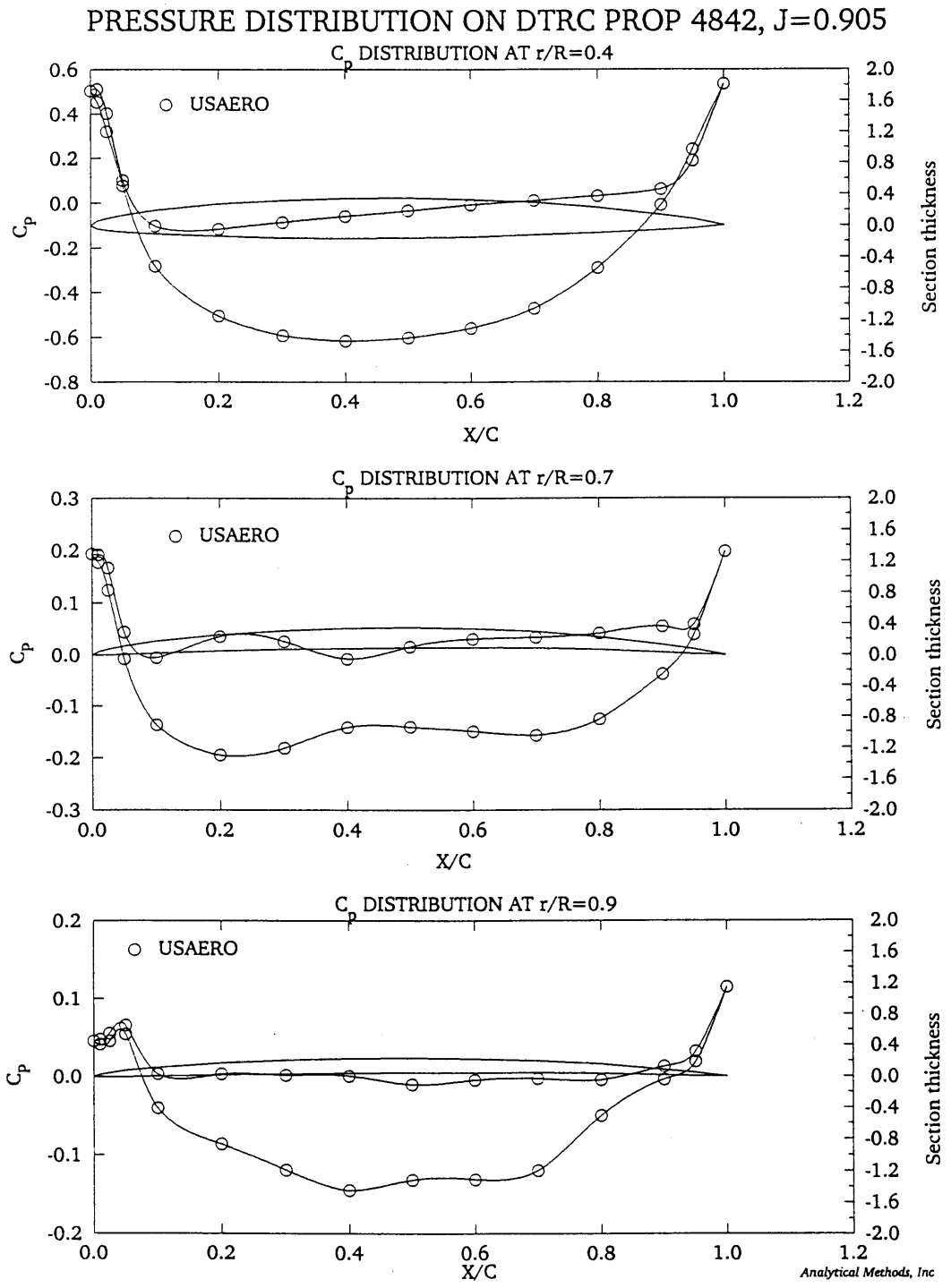

Fig. 4.10. Calculated Chordwise Pressure Distributions by USAERO at Three Radial Stations at J = 0.905.

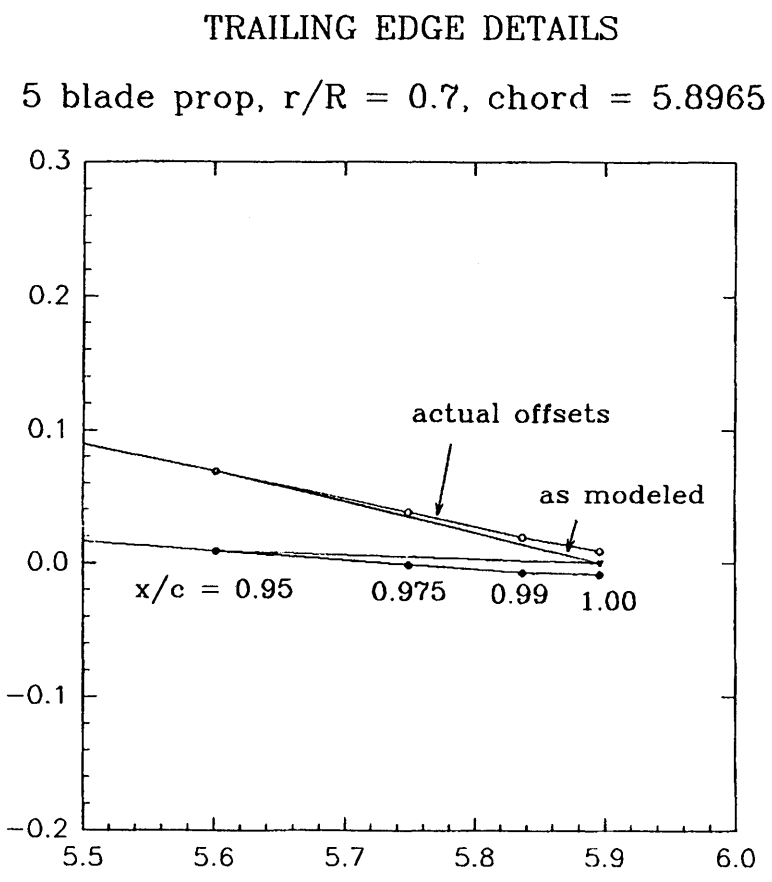

Fig. 4.11. Details of Trailing Edge Modification for Sharp Edge.

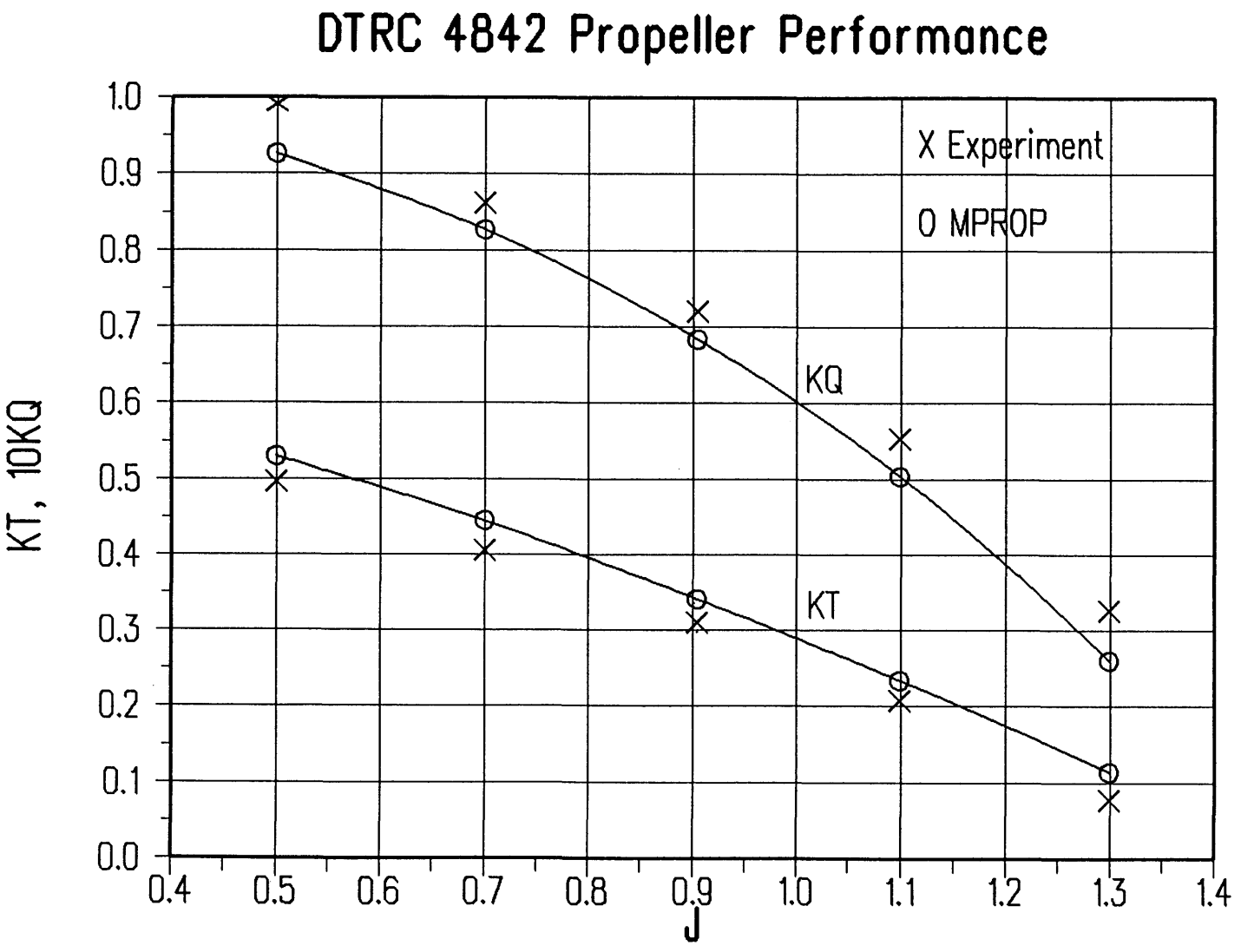

Fig. 4.12. Comparison of Calculated and Experimental KT, KQ Characteristics Using VSAERO/MPROP.

Fig. 4.13. Calculated Skin Friction Distribution at J = 0.905
(a) Along Streamlines in VSAERO/MPROP.

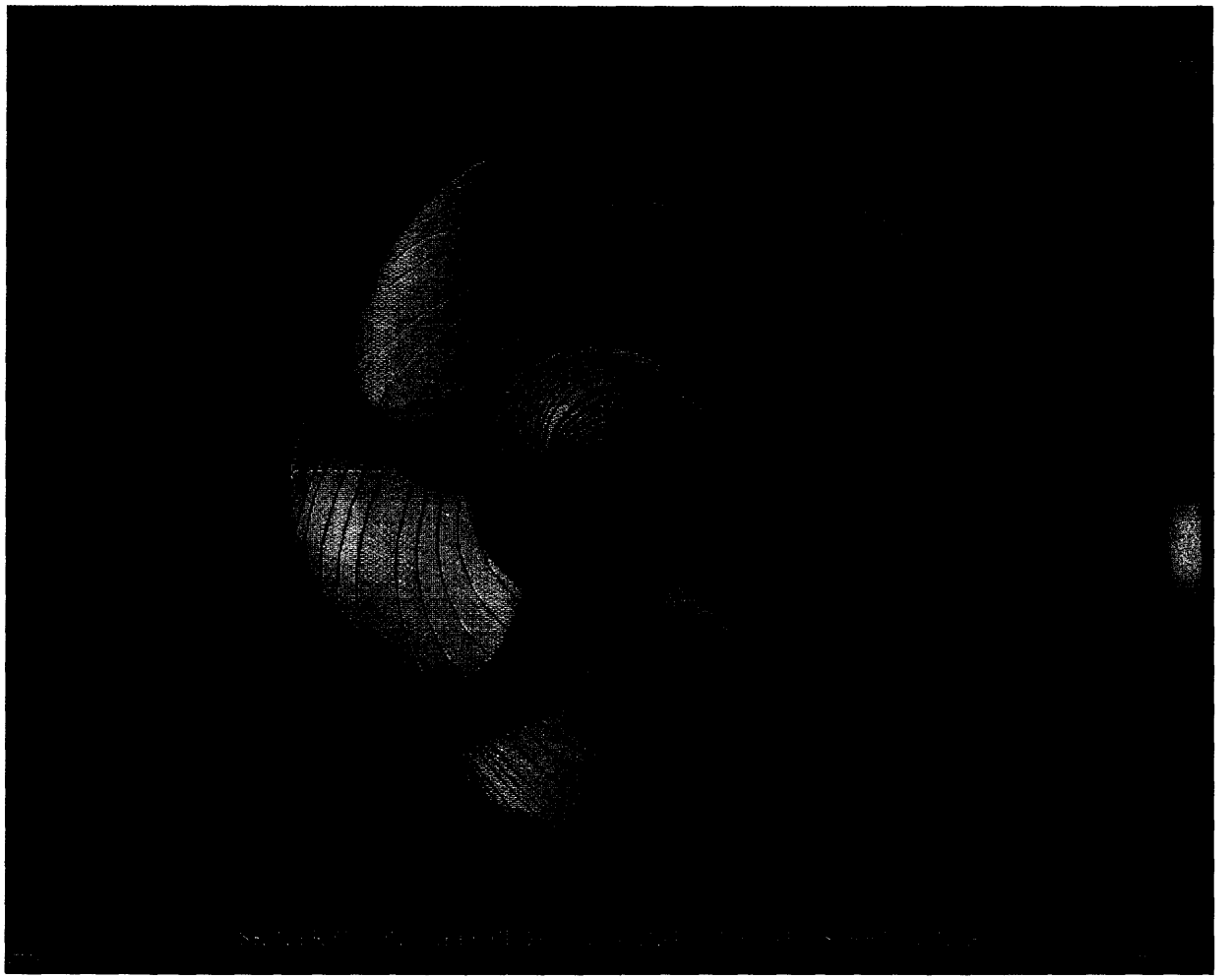

Fig. 4.13 Continued.
(b) Along Streamlines in USAERO.